P1.45 ASSESSMENT OF A COUPLED MOMENTUM AND PASSIVE SCALAR FLUX SUBGRID-SCALE TURBULENCE MODEL FOR LARGE-EDDY SIMULATION OF FLOW IN THE PLANETARY BOUNDARY LAYER

Rica Mae Enriquez*, Robert L. Street, Francis L. Ludwig
Stanford University, Stanford, CA

1. ABSTRACT

We previously developed a linear algebraic subgrid-scale stress [LASS] model. In this paper, we extend our previous work to be applicable to a range of atmospheric stability conditions for the dry atmosphere by adding a passive algebraic subgrid-scale [SGS] heat flux model, which includes scalar production and pressure redistribution terms. We apply this generalized LASS [GLASS] model to large-eddy simulations of idealized atmospheric convective and stable boundary layers. For both boundary layer cases, GLASS predicts the evolution of resolved and SGS turbulent quantities at least as well as the LESs with diffusion models, while including additional physics.

2. A COUPLED SGS TURBULENCE MODEL

Our linear algebraic subgrid-scale stress [LASS] model includes production, dissipation, and pressure redistribution terms (see Enriquez et al., 2010a; Enriquez et al., 2010b, for more details on our strategy and approach). Here, we extend our previous work to be applicable to a range of atmospheric stability conditions for the dry atmosphere by adding a passive algebraic subgrid-scale heat flux model, which includes scalar production and pressure redistribution terms. In what follows the SGS terms are:

1) stress, $\bar{A}_{ik} = \overline{\widetilde{u_i u_k}} - \overline{\tilde{u}_i \tilde{u}_k}$, and
2) heat flux, $\bar{a}_i = \overline{\widetilde{u_i \theta}} - \overline{\tilde{u}_i \tilde{\theta}}$,

where, in the Carati et al. (2001) framework for LES, the overbar represents a spatial filter and the tilde represents a discretization filter. In this paper we focus only on the SGS model, ignoring reconstruction effects; see (Enriquez et al., 2010a) for an application with SGS and reconstruction models together.

2.1 *The Linear Algebraic Subgrid-Scale Stress [LASS] Model*

The evolution equation of the SGS stress, A_{ik}, includes: advection, diffusion, production, dissipation, pressure redistribution, buoyancy generation, and Coriolis terms. We simplify the equation to be modeled to include only production, dissipation, and pressure redistribution; neglected terms are assumed small. Production terms are not modeled, the dissipation term appears in its general isotropic form for high Reynolds number flows, and the pressure redistribution term is modeled with the Reynolds-averaged Navier-Stokes Launder et al. (1975) model adopted for LES.

$$0 = \underbrace{-\bar{A}_{jk}\frac{\partial \bar{\tilde{u}}_i}{\partial x_k} - \bar{A}_{ik}\frac{\partial \bar{\tilde{u}}_j}{\partial x_k}}_{\text{Mean-Gradient Production}} \underbrace{-\tfrac{2}{3}\bar{\varepsilon}\delta_{ij}}_{\text{Dissipation}} \underbrace{+\Pi_{ij,LASS}}_{\text{Pressure Redistribution}} \quad (1)$$

The pressure redistribution, $\Pi_{ij,LASS}$, is collectively a slow pressure-strain term, a rapid pressure-strain term, and a wall effects term that involves interactions of the first two terms and a surface:

$$\begin{aligned}\Pi_{ij,LASS} = &\underbrace{-c_1\frac{\bar{\varepsilon}}{\bar{e}}\left(\bar{A}_{ij} - \tfrac{2}{3}\bar{e}\delta_{ij}\right)}_{\text{Slow Pressure Strain}} \\ &\underbrace{-c_2\left(P_{ij} - \tfrac{2}{3}P\delta_{ij}\right) - c_3\bar{e}\bar{\tilde{S}}_{ij} - c_4\left(D_{ij} - \tfrac{2}{3}P\delta_{ij}\right)}_{\text{Rapid Pressure Strain}} \\ &\underbrace{+\left(c_5\frac{\bar{\varepsilon}}{\bar{e}}\left(\bar{A}_{ij} - \tfrac{2}{3}\bar{e}\delta_{ij}\right) + c_6 P_{ij} - c_7 D_{ij} + c_8\bar{e}\bar{\tilde{S}}_{ij}\right)f(h)}_{\text{Wall Effects}}\end{aligned} \quad (2)$$

With Equations (1) – (2) the following equations form the LASS model:

$$P_{ij} = -\left(\bar{A}_{ik}\frac{\partial \bar{\tilde{u}}_j}{\partial x_k} + \bar{A}_{jk}\frac{\partial \bar{\tilde{u}}_i}{\partial x_k}\right) \quad (3)$$

$$P = -\bar{A}_{ij}\frac{\partial \bar{\tilde{u}}_j}{\partial x_i} \quad (4)$$

$$\bar{\tilde{S}}_{ij} = \left(\frac{\partial \bar{\tilde{u}}_i}{\partial x_k} + \frac{\partial \bar{\tilde{u}}_k}{\partial x_i}\right) \quad (5)$$

$$\bar{\tilde{S}}^2 = \frac{1}{2}\bar{\tilde{S}}_{ij}\bar{\tilde{S}}_{ij} \quad (6)$$

$$D_{ij} = -\left(\bar{A}_{ik}\frac{\partial \bar{\tilde{u}}_k}{\partial x_j} + \bar{A}_{jk}\frac{\partial \bar{\tilde{u}}_k}{\partial x_i}\right) \quad (7)$$

$$\triangle_g = \left(\triangle_x\triangle_y\triangle_z\right)^{1/3} \quad (8)$$

$$f(h) = 0.27\frac{\triangle_g}{h} \quad (9)$$

$$\bar{e} = \tfrac{1}{2}\bar{A}_{ii} \quad (10)$$

$$\bar{\varepsilon} = 1.2\frac{\bar{e}^{1.5}}{\triangle_g} \quad (11)$$

* *Corresponding author address*: Rica Mae Enriquez, Stanford University, Civil & Environmental Engineering Department, Stanford, CA, 94305; ricae@stanford.edu

Model coefficients [Table 1] are based on suggestions from Launder et al. (1975), Morris (1984), Shabbir and Shih (1992), and Wallin and Johansson (2000). We strongly emphasize that a canopy wall model ***is not*** used.

Table 1. LASS model coefficients

c_1	c_2	c_3	c_4	c_5	c_6	c_7	c_8
1.8	0.78	0.27	0.22	0.8	0.06	0.06	0.0

Results of large-eddy simulations at various resolutions of a neutrally-stratified boundary layer flow over a flat, rough surface indicate that the LASS model is a more physically complete SGS stress turbulence model that provides near-wall anisotropies that eddy-viscosity models do not, and yields proper shear stress values in the logarithmic layer. We have also examined the combination of the LASS model with reconstruction, using the approximate deconvolution model, of the subfilter-scale stress (Chow et al., 2005). With that mixed model we are able to represent both anisotropy and energy backscatter (Enriquez et al., 2010a).

2.2 *The Generalized Linear Algebraic Subgrid-Scale Stress [GLASS] Model*

The SGS stresses are solved as a system of linear equations as above and are then coupled to the set of equations that model the SGS heat flux. The fully coupled active scalar version of the GLASS model includes a buoyant production term:

$$0 = \underbrace{-\bar{A}_{jk}\frac{\partial \bar{\bar{u}}_i}{\partial x_k} - \bar{A}_{ik}\frac{\partial \bar{\bar{u}}_j}{\partial x_k}}_{\text{Mean-Gradient Production}} \underbrace{-\tfrac{2}{3}\bar{\varepsilon}\delta_{ij}}_{\text{Dissipation}} \underbrace{+\Pi_{ij,GLASS}}_{\text{Pressure Redistribution}} \underbrace{\cancel{+\frac{g}{\theta_o}\left(\bar{a}_j\delta_{i3} + \bar{a}_i\delta_{j3}\right)}}_{\text{Buoyant Production}} \qquad (12)$$

and the rapid pressure strain term of Equation (2) has an additional corresponding buoyancy production term:

$$\Pi_{ij,GLASS} = \Pi_{ij,LASS} \cancel{-c_g\frac{g}{\theta_o}\left(\bar{a}_j\delta_{i3} + \bar{a}_i\delta_{j3} - \tfrac{2}{3}\bar{a}_3\delta_{i3}\delta_{ij}\right)} \, . \qquad (13)$$

In this paper, the buoyant production terms are left out, as indicated by the crossed out terms above, and we are modeling SGS heat flux as a passive scalar, which is, however, influenced by the SGS stress acting on the mean temperature gradient.

The evolution equation of the SGS heat flux includes: advection, diffusion, gradient production, viscosity, pressure redistribution, buoyancy production, and Coriolis terms. We simplify the equation to be modeled to include only production, dissipation, and pressure redistribution. Buoyant production is neglected as Ramachandran and Wyngaard (2010) showed it to be small compared to other terms; other neglected terms are also assumed small. Production terms are not modeled, the dissipation term drops out, and the pressure redistribution term is modeled with the Reynolds-averaged Navier-Stokes Launder and Samaraweera (1979) model:

$$0 = \underbrace{-\bar{A}_{ik}\frac{\partial \bar{\bar{\theta}}}{\partial x_k} - \bar{a}_k\frac{\partial \bar{\bar{u}}_i}{\partial x_k}}_{\text{Mean-Gradient Production}} \underbrace{+\Pi_{i\theta}}_{\text{Pressure Redistribution}} \qquad (14)$$

$$\Pi_{i\theta} = \underbrace{-c_{1\theta}\frac{\bar{\varepsilon}}{\bar{e}}\bar{a}_i}_{\text{Slow Pressure Strain}} \underbrace{+c_{2\theta}\bar{a}_k\frac{\partial \bar{\bar{u}}_i}{\partial x_k}}_{\text{Rapid Pressure Strain}} \underbrace{-c_{3\theta}\frac{\bar{\varepsilon}}{\bar{e}}\bar{a}_i\, f(h)}_{\text{Wall Effects}} \qquad (15)$$

For this model, we account for stability and shear by modifying 1) the SGS TKE term and 2) the dissipation term by altering its length scale according to Deardorff (1980):

$$\bar{e} = \begin{cases} \tfrac{1}{2}\bar{A}_{ii} & \text{if } \tfrac{1}{2}\bar{A}_{ii} > 0.0, \\ 0.0826\triangle_g^2\bar{\tilde{S}}^2 & \text{if } \tfrac{1}{2}\bar{A}_{ii} == 0.0 \text{ and } N^2 \le 0.0. \end{cases} \qquad (16)$$

$$N^2 = \frac{g}{\theta}\frac{\partial \theta}{\partial z} \qquad (17)$$

$$\triangle_B = \begin{cases} 0.76\sqrt{\frac{\bar{e}}{N^2}} & \text{if } N^2 > 0.0, \\ \triangle_g & \text{if } N^2 \le 0.0, \end{cases} \qquad (18)$$

$$\bar{\varepsilon} = 1.2\frac{\bar{e}^{1.5}}{\triangle_B} \qquad (19)$$

We refer to the set of SGS stress-heat flux equations as the GLASS model. Model coefficients [Table 2] are based on suggestions from Launder and Samaraweera (1979), Chen and Jaw (1998), Wikstrom et al. (2000), and Craft and Launder (2001).

Table 2. GLASS model coefficients

$c_{1\theta}$	$c_{2\theta}$	$c_{3\theta}$	c_g
3.0	0.5	0.0	0.5

3. LES SETUP AND RESULTS

We employ the Advanced Regional Prediction System [ARPS] in LES mode (cf., Chow et al., 2005; Enriquez et al., 2010a). ARPS is 3D, compressible, non-hydrostatic, and parallelized (Doyle et al., 2000; Xue et al., 2000; Xue et al., 2001; Chow et al., 2005). As usual in LES, the governing equations are filtered and ARPS generates the resolved-scale flow variables as influenced by the SGS terms discussed above, as well as the output from the SGS subroutines. See Enriquez et al. (2010a, 2010b) for more details of the setup and processes.

We test GLASS with different stability conditions with simulations of a convective and stable boundary layer. Details of the simulations and the results of the two simulations are described in the following subsections.

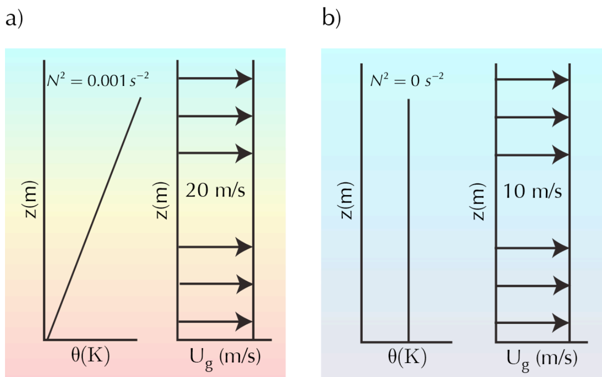

Figure 1. LES initial conditions for the convective (a) and stable (b) boundary layers.

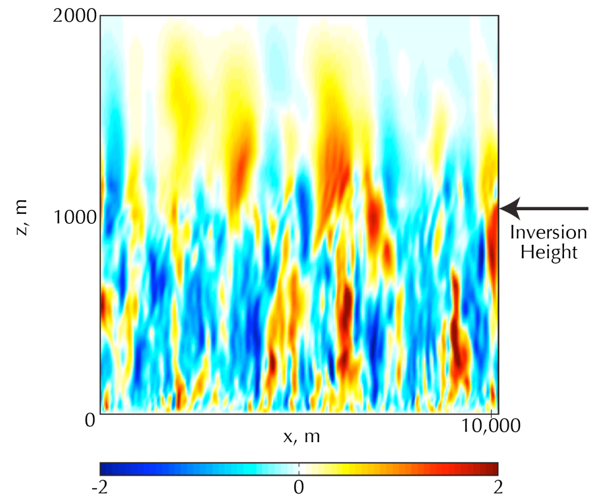

Figure 2. Instantaneous resolved vertical velocity x-z slice (y = 5,120 m) at 10,000 s. The varied length scales can be seen, from meters by the surface to hundreds of meters near and above the inversion.

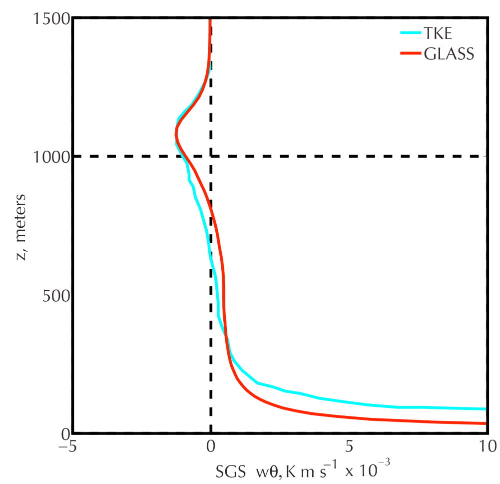

Figure 3. Subgrid-scale vertical heat flux at 10,000 s for simulations using the TKE-1.5 and GLASS turbulence models.

3.1 *Convective Boundary Layer [CBL] Flow*

We simulate a surface sheared CBL with a constant geostrophic wind of 20 m s^{-1} (Fedorovich, 2004; Conzemius and Fedorovich, 2006; Fedorovich and Conzemius, 2008). Initial conditions of the simulation can be seen in Figure 1a and LES parameters are listed in Table 3. Simulations are carried out for 10,000 s, before the upper damping layer clearly impacts the CBL.

Table 3. Convective boundary layer LES parameters

Horizontal resolution, Δ_x,Δ_y	40 m
Vertical resolution, Δ_z	20 m average, 10 m minimum
Domain size	10.24 km x 10.24 km x 2 km
Time steps	0.5 s large, 0.05 s small
Reference temperature	300 °K
Surface heat flux	0.1 °K m s^{-1}
Coriolis parameter	f [40° N] = 0.9 x 10^{-4} s^{-1}
Lateral boundaries	Periodic
Bottom boundary	Rigid wall, semi-slip
Roughness length	0.01 m

Turbulence occurs at various scales in the CBL. Small-scale turbulence dominates in the surface layer, while large thermals play a key role in the mixed layer. Instantaneous resolved vertical velocity x-z slice at 10,000 s [Figure 2] shows that varied length scales can be seen, from tens of meters by the surface to hundreds of meters near and above the inversion, in the simulation using the GLASS turbulence model.

In addition, in Figure 3 we compare the planar averaged ARPS SGS heat flux vertical profile produced by GLASS with the ARPS SGS heat flux vertical profile produced by a turbulent kinetic energy [TKE]-1.5 turbulence closure (Deardorff, 1980) at 10,000 s (Fedorovich, 2004). For this simulation, we see that these averaged SGS heat flux profiles are similar in magnitude and shape, and have a negative peak in close proximity to the inversion height. It is important to note that the SGS heat flux is a very small part of the total heat flux.

One of the most notable contributions of the LASS model is its ability to provide near-wall SGS stress anisotropy. In addition to near-wall stress anisotropy, GLASS represents the SGS heat flux anisotropy for wall-bounded flows that isotropic eddy diffusion models cannot because the SGS heat fluxes are not, in general, aligned with the resolved scalar gradient. The heat transport in the temperature field of wall-bounded shear flows is known to be anisotropic at inertial and dissipative scales (Warhaft, 2000). Figure 4 depicts the GLASS planar averaged SGS heat fluxes, at 10,000 s.

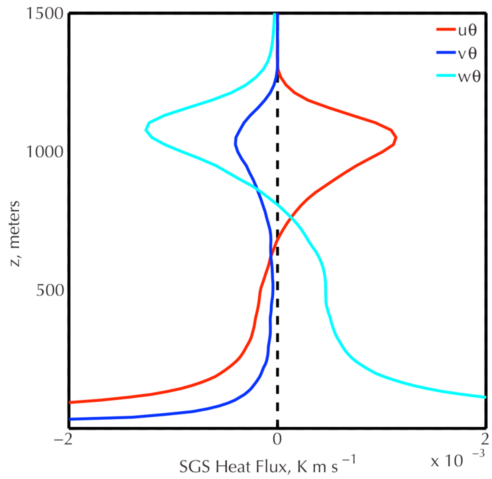

Figure 4. GLASS planar and time averaged SGS heat fluxes, at 10,000 s.

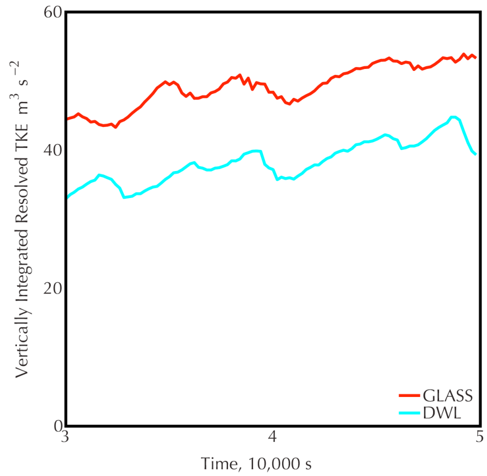

Figure 5. GLASS and Dynamic Wong-Lilly [DWL] simulations maintain a high level of vertically integrated SGS turbulent kinetic energy.

3.2 *Stable Boundary Layer [SBL] Flow*

We simulated a moderately stable atmospheric boundary layer driven by a geostrophic wind of 10 m s^{-1} at a coarse resolution (Zhou and Chow, 2011). Initial conditions of the simulation can be seen in Figure 1b and LES parameters are listed in Table 4. Similar simulations at higher resolutions have been conducted by Kosović and Curry (2000), Saiki et al. (2000), Basu and Porté-Agel (2006).

Table 4. Stable boundary layer LES parameters

Horizontal resolution, Δ_x,Δ_y	16 m
Vertical resolution, Δ_z	16 m average, 5 m minimum
Domain size	640 m x 640 m x 640 m
Time steps	0.25 s large, 0.025 s small
Initial surface temperature	300 °K
Surface heat flux	-0.02 °K m s^{-1}
Coriolis parameter	f [45° N] = 1 x 10^{-4} s^{-1}
Lateral boundaries	Periodic
Bottom boundary	Rigid wall, semi-slip
Roughness length	0.1 m

We carry out our simulations for 50,000 s to demonstrate that GLASS sustains resolved turbulent kinetic energy at a coarse resolution. It is evident that at this coarse resolution of 16 m, the Dynamic Wong-Lilly (Wong and Lilly, 1994) SGS turbulence model [DWL] and GLASS sustain the resolved TKE throughout the simulation [Figure 5]. The resolved TKE decayed rapidly in similar simulations that used non-dynamic eddy-viscosity turbulence models, like the Smagorinsky and TKE-1.5 (Zhou and Chow, 2011). We use DWL results to compare the performance of GLASS to a dynamic eddy-viscosity model and to the results of Zhou and Chow (2011).

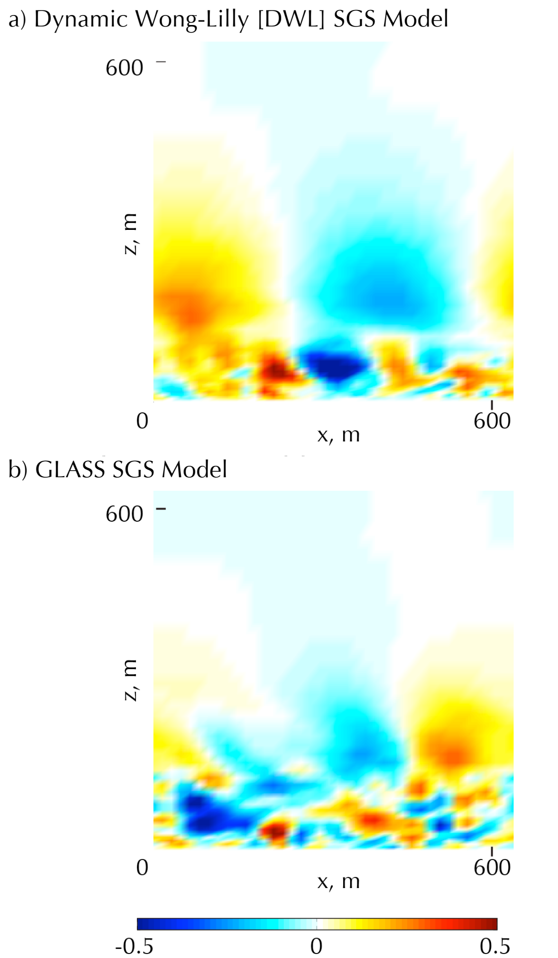

Figure 6. Instantaneous resolved vertical velocity x-z slices (y = 320 m) of two different SGS turbulence models at 50,000 s.

The vertical slices of the instantaneous resolved vertical velocity of the DWL [Figure 6a] and the GLASS [Figure 6b] models highlight the difference of CBL and SBL dynamics. In the SBL, the range of scales is smaller and the turbulence is concentrated near the surface. In addition, these figures underscore that turbulence in this regime is a delicate dynamical balance between buoyancy and shear, and different SGS parameterizations can produce different results. The GLASS model appears to produce smaller structures than DWL near the surface and at higher elevations.

The planar and time averaged horizontal velocity profiles [Figure 7] reveal that the DWL predicts a low-level jet at a slightly lower elevation than GLASS. This indicates that GLASS predicts a deeper SBL. Similarly, Zhou and Chow (2011) demonstrate that their dynamic reconstruction model, which models more physical turbulent processes, also predicts a deeper SBL than a TKE-1.5 model.

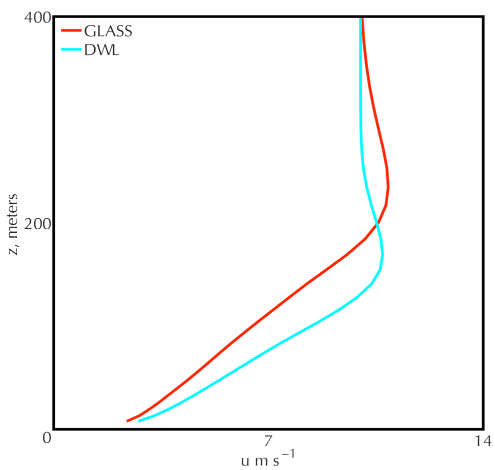

Figure 7. Horizontally and time-averaged (40,000 – 50,000 s) vertical profiles for horizontal velocity, u.

4. CONCLUSIONS

The CBL and SBL simulations demonstrate that GLASS can 1) perform well at different stability regimes and 2) provide scalar and momentum flux anisotropies. Notably, GLASS overcomes the need to alter model coefficients for different positions in the flow, grid/filter aspect ratios, and atmospheric stabilities, etc. Future work includes adding the buoyancy production terms for two-way coupling and simulating a diurnal cycle to study the transitions from one stability case to another.

5. ACKNOWLEDGMENTS

We appreciate our helpful discussions with Professor Tina Chow and Dr. Bowen Zhou of UC Berkeley and Dr. Peter Sullivan of NCAR. We are grateful to NCAR for allocation of computer time used in this research. This material is based upon work supported by the National Science Foundation under Grant No. 1001262.

6. REFERENCES

Basu, S., and F. Porté-Agel, 2006: Large-eddy simulation of stably stratified atmospheric boundary layer turbulence: A scale-dependent dynamic modeling approach. *Journal of the Atmospheric Sciences*, **63,** 2074-2091.

Carati, D., G. S. Winckelmans, and H. Jeanmart, 2001: On the modelling of the subgrid-scale and filtered-scale stress tensors in large-eddy simulation. *Journal of Fluid Mechanics*, **441,** 119-138.

Chen, C.-J., and S.-Y. Jaw, 1998: *Fundamentals of turbulence modeling.* Taylor and Francis.

Chow, F. K., R. L. Street, M. Xue, and J. H. Ferziger, 2005: Explicit filtering and reconstruction turbulence modeling for large-eddy simulation of neutral boundary layer flow. *Journal of the Atmospheric Sciences*, **62,** 2058-2077.

Conzemius, R. J., and E. Fedorovich, 2006: Dynamics of sheared convective boundary layer entrainment. Part I: Methodological background and large-eddy simulations. *Journal of the Atmospheric Sciences*, **63,** 1151-1178.

Craft, T. J., and B. E. Launder, 2001: Principles and performance of TCL-based second-moment closures. *Flow, Turbulence and Combustion*, **66,** 355-372.

Deardorff, J. W., 1980: Stratocumulus-capped mixed layers derived from a three-dimensional model. *Boundary-Layer Meteorology*, **18,** 495-527.

Doyle, J. D., D. R. Durran, C. Chen, B. A. Colle, M. Georgelin, V. Grubisic, W. R. Hsu, C. Y. Huang, D. Landau, Y. L. Lin, G. S. Poulos, W. Y. Sun, D. B. Weber, M. G. Wurtele, and M. Xue, 2000: An intercomparison of model-predicted wave breaking for the 11 January 1972 Boulder windstorm. *Monthly Weather Review*, **128,** 901-914.

Enriquez, R. M., F. K. Chow, R. L. Street, and F. L. Ludwig, 2010a: Examination of the linear algebraic subgrid-scale stress [LASS] model, combined with reconstruction of the subfilter-scale stress, for large-eddy simulation of the neutral atmospheric boundary layer. 19th Symposium on Boundary Layers and Turbulence, Keystone, CO, American Meteorological Society, Paper 3A.3, 8 pp.

Enriquez, R. M., R. L. Street, and F. L. Ludwig, 2010b: Algebraic subgrid-scale turbulence modeling in large-eddy simulation of the atmospheric boundary layer. The 5th International Symposium on Computational Wind Engineering, Chapel Hill, NC, International Association for Wind Engineering, Paper 154, 8 pp.

Fedorovich, E., and R. Conzemius, 2008: Effects of wind shear on the atmospheric convective

boundary layer structure and evolution. *Acta Geophysica*, **56,** 114-141.
Fedorovich, E., R. Conzemius, I. Esau, F. Katopodes Chow, D. Lewellen, C.-H. Moeng, D. Pino, P. Sullivan, and J. Vilà-Guerau De Arellano, 2004: Entrainment into sheared convective boundary layers as predicted by different large eddy simulation codes. 16th Symposium on Boundary Layers and Turbulence, Portland, ME, American Meteorological Society, Paper P4.7.
Kosović, B., and J. A. Curry, 2000: A large eddy simulation study of a quasi-steady, stably stratified atmospheric boundary layer. *Journal of the Atmospheric Sciences*, **57,** 1052-1068.
Launder, B. E., G. J. Reece, and W. Rodi, 1975: Progress in the development of a Reynolds-stress turbulence closure. *Journal of Fluid Mechanics*, **68,** 537-566.
Launder, B. E., and D. S. A. Samaraweera, 1979: Application of a second-moment turbulence closure to heat and mass transport in thin shear flows—I. Two-dimensional transport. *International Journal of Heat and Mass Transfer*, **22,** 1631-1643.
Morris, P. J., 1984: Modeling the pressure redistribution terms. *Physics of Fluids*, **27,** 1620-1623.
Ramachandran, S., and J. Wyngaard, 2010: Subfilter-scale modelling using transport equations: Large-eddy simulation of the moderately convective atmospheric boundary layer. *Boundary-Layer Meteorology***,** 1-35.
Saiki, E. M., C.-H. Moeng, and P. P. Sullivan, 2000: Large-eddy simulation of the stably stratified planetary boundary layer. *Boundary-Layer Meteorology*, **95,** 1-30.
Shabbir, A., and T. H. Shih, 1992: Critical assessment of Reynolds stress turbulence models using homogeneous flows. NASA TM 105954I, COMP-92-24, CMOTT-92-12.
Wallin, S., and A. V. Johansson, 2000: An explicit algebraic Reynolds stress model for incompressible and compressible turbulent flows. *Journal of Fluid Mechanics*, **403,** 89-132.
Warhaft, Z., 2000: Passive scalars in turbulent flows. *Annual Review of Fluid Mechanics*, **32,** 203-240.
Wikstrom, P. M., S. Wallin, and A. V. Johansson, 2000: Derivation and investigation of a new explicit algebraic model for the passive scalar flux. *Physics of Fluids*, **12,** 688-702.
Wong, V. C., and D. K. Lilly, 1994: A comparison of two dynamic subgrid closure methods for turbulent thermal convection. *Physics of Fluids*, **6,** 1016-1023.
Xue, M., K. K. Droegemeier, and V. Wong, 2000: The Advanced Regional Prediction System (ARPS) - A multi-scale nonhydrostatic atmospheric simulation and prediction model. Part I: Model dynamics and verification. *Meteorology and Atmospheric Physics*, **75,** 161-193.
Xue, M., K. K. Droegemeier, V. Wong, A. Shapiro, K. Brewster, F. Carr, D. Weber, Y. Liu, and D. Wang, 2001: The Advanced Regional Prediction System (ARPS) - A multi-scale nonhydrostatic atmospheric simulation and prediction tool. Part II: Model physics and applications. *Meteorology and Atmospheric Physics*, **76,** 143-165.
Zhou, B., and F. K. Chow, 2011: Large-eddy simulation of the stable boundary layer with explicit filtering and reconstruction turbulence modeling. *Journal of the Atmospheric Sciences*, **68,** 2142-2155.